

LEARNING DIRECTED ACYCLIC GRAPHS WITH HIDDEN VARIABLES VIA LATENT GAUSSIAN GRAPHICAL MODEL SELECTION

BENJAMIN FROT, PREETAM NANDY, AND MARLOES H. MAATHUIS

ABSTRACT. We introduce a new method to estimate the Markov equivalence class of a directed acyclic graph (DAG) in the presence of hidden variables, in settings where the underlying DAG among the observed variables is sparse, and there are a few hidden variables that have a direct effect on many of the observed ones. Building on the so-called low rank plus sparse framework, we suggest a two-stage approach which first removes unwanted variation using latent Gaussian graphical model selection, and then estimates the Markov equivalence class of the underlying DAG by applying GES. This approach is consistent in certain high-dimensional regimes and performs favourably when compared to the state of the art, both in terms of graphical structure recovery and total causal effect estimation.

1. INTRODUCTION

The task of learning directed acyclic graphs (DAGs) arises in many areas of science and engineering. In such graphs, nodes represent random variables and edges encode conditional dependencies. The problem of recovering their structure from observational data is challenging and cannot be tackled without making untestable assumptions [33]. Among other assumptions, *causal sufficiency* is particularly constraining. Briefly, causal sufficiency requires that there be no hidden (or latent) variables that are common causes of two or more observed variables (such hidden variables are often called *confounders*). Although causal sufficiency is unrealistic in most applications, many structure learning algorithms operate under this assumption [40, 7, 43, 17, 31]. On the other hand, methods allowing for arbitrary hidden structures tend to be overly conservative, recovering only a small subset of the causal effects [41, 10, 8, 29]. In the present work, we suggest taking a middle-ground stance on causal sufficiency by allowing hidden variables while imposing some restrictions on their number and behaviour. More precisely, we consider settings where the underlying DAG among the observed variables is sparse, and there are a few hidden variables that have a direct effect on many of the observed ones [6]. This is an interesting problem for at least two reasons.

First, these assumptions cover important real-world applications. In the context of gene expression data, for example, such confounding occurs due to technical factors or unobserved environmental variables [25, 42, 16]. For another example, consider the task of modelling the inverse covariance structure of stock returns [21,

Date: November 19, 2018.

Key words and phrases. directed acyclic graph (DAG), high-dimensional data, causal inference, hidden variables, low-rank plus sparse.

BF and PN are equally contributing authors.

§9.5]. [6] showed that a large fraction of the conditional dependencies among stock returns can be explained by a few hidden variables, *e.g.* energy prices.

Second, this setting is complementary to the realm of application of popular algorithms that do not assume causal sufficiency, such as versions of the Fast Causal Inference algorithm [41, 10, 8]. Under our assumptions, most observed variables do not appear conditionally independent of each other and the underlying so-called *maximal ancestral graph* is expected to be dense which, in turn, implies that very few causal effects are identifiable and bounded away from zero (see Figure 1 for an example). Moreover, learning such dense graphs is computationally demanding.

In this paper, we suggest a two-stage procedure. First, the so-called “low-rank plus sparse” approach of [6] is used to obtain a pair of inverse covariance matrices, (\hat{S}, \hat{L}) say, describing the estimated Gaussian graphical model over the observed variables and the estimated effect of the hidden variables, respectively. In the second stage, a causal structure learning algorithm which assumes causal sufficiency is applied to \hat{S}^{-1} . In addition, (joint) total causal effects can be straightforwardly estimated using the (joint-)IDA algorithm [28, 27, 32].

The suggested approach is conceptually simple and enjoys many desirable theoretical and computational properties. In particular, we derive conditions under which this estimator is consistent in a high-dimensional regime. Through extensive simulations, we show that our approach outperforms other relevant methods, both in terms of graph structure recovery and total causal effect estimation. Our main focus being on applicability, we also suggest strategies to select the tuning parameters in various settings and illustrate their performances in simulations. Finally, we analyse two datasets. In our first application, we model the expression levels of the genes responsible for isoprenoid synthesis in *Arabidopsis thaliana* and show that some of the hidden variables we estimate have a clear biological interpretation. We also model the expression levels of hundreds of genes expressed in ovarian cancer and assess our results using two external sources of validation. Compared to state-of-the-art algorithms, we find our approach to be better at recovering known causal relationships¹.

2. PROBLEM STATEMENT

2.1. Graphical Models Terminology. We consider graphs $\mathcal{G} = (X, E)$, where the vertices (or nodes) $X = \{X_1, X_2, \dots\}$ represent random variables and the edges represent relationships between pairs of variables. The edges can be either *directed* ($X_i \longrightarrow X_k$) or *undirected* ($X_i \circ\text{---}\circ X_k$). An *(un)directed graph* can only contain (un)directed edges, whereas a *partially directed graph* may contain both directed and undirected edges. The *skeleton* of a partially directed graph \mathcal{G} , denoted as $\text{skeleton}(\mathcal{G})$, is the undirected graph that results from replacing all directed edges of \mathcal{G} by undirected edges. Two nodes X_i and X_k are *adjacent* if there is an edge between them. If $X_i \longrightarrow X_k$, then X_i is a *parent* of X_k . A *path* between X_i and X_k in a graph \mathcal{G} is a sequence of distinct nodes (X_i, \dots, X_k) such that all pairs of successive nodes in the sequence are adjacent in \mathcal{G} . A *directed path* from X_i to X_k is a path between X_i and X_k , where all edges are directed towards X_k . A directed path from X_i to X_k together with $X_k \longrightarrow X_i$ forms a *directed cycle*. A graph without directed cycles is *acyclic*. A graph that is both (partially) directed and acyclic, is a *(partially) directed acyclic graph* or (P)DAG.

¹The code for our simulations and applications is made available with this paper.

A DAG encodes conditional independence relationships via the notion of *d-separation* [see 34, Def. 1.2.3]. Several DAGs can encode the same d-separations and such DAGs form a *Markov equivalence class*. A Markov equivalence class of DAGs can be uniquely represented by a *completed partially directed acyclic graph* (CPDAG), which is a PDAG that satisfies the following: $X_i \longrightarrow X_k$ in the CPDAG if $X_i \longrightarrow X_k$ in every DAG in the Markov equivalence class, and $X_i \circ\text{---} X_k$ in the CPDAG if the Markov equivalence class contains a DAG in which $X_i \longrightarrow X_k$ as well as a DAG in which $X_i \longleftarrow X_k$ [44, 3].

For $S \subseteq X \setminus \{X_i, X_j\}$, we write $X_i \perp\!\!\!\perp X_j | S$ to denote conditional independence in the joint distribution of X , while $X_i \perp_{\mathcal{G}} X_j | S$ means that X_i and X_j are d-separated by S in \mathcal{G} . A DAG \mathcal{G} is a *perfect map* of the joint distribution of X if for all X_i, X_j such that $X_i \neq X_j$ and for all $S \subseteq X \setminus \{X_i, X_j\}$, we have $X_i \perp\!\!\!\perp X_j | S \Leftrightarrow X_i \perp_{\mathcal{G}} X_j | S$.

When some variables are unobserved, as is assumed in this paper, complications arise because the class of DAGs is not closed under marginalisation. Among other factors, this limitation prompted the development of another class of graphical independence models called *maximal ancestral graphs* (MAGs) [37]. A criterion akin to d-separation makes it possible to read-off independencies of such graphs and, since multiple MAGs can encode the same set of conditional independence statements, one usually attempts to recover a *partial ancestral graph* (PAG) which describes a Markov equivalence class of MAGs [2]. Like in CPDAGs, circle marks represent uncertainty about edge marks. In particular, a circle mark occurs in the PAG if the Markov equivalence class contains a MAG in which the edge mark is a tail, and a MAG in which the edge mark is an arrowhead [46].

2.2. Setup and Notations. Throughout, we assume that we are given n independent, identically distributed (i.i.d.) realisations of a partially observed zero-mean random vector $X = (X_O^T, X_H^T)^T \in \mathbb{R}^{p+h}$. The subvector $X_H \in \mathbb{R}^h$ corresponds to those variables that remain hidden. Our main assumptions are *a)* X is normally distributed and *b)* there exists a DAG, \mathcal{G}_O^* say, which is a perfect map of the distribution of X_O conditional on X_H . While our initial motivation came from causal problems, as discussed in the introduction, our assumptions do not require \mathcal{G}_O^* to be the causal DAG. Moreover, we do not assume that X_H is generated by a linear Gaussian DAG, a scenario which arises as a special case.

More formally, our first assumption amounts to saying that the distribution of X is of the form $X \sim \mathcal{N}(0, K^{*-1})$ with inverse covariance (or *precision*) matrix K^* given by

$$K^* := \begin{pmatrix} K_O^* & K_{HO}^{*T} \\ K_{HO}^* & K_H^* \end{pmatrix}.$$

The superscript \cdot^* is used to indicate that these matrices are parameters of the model, as opposed to estimates. Moreover, we make use of partitioned matrices, so that $K_O^* \in \mathbb{R}^{p \times p}$, $K_{HO}^* \in \mathbb{R}^{h \times p}$ and $K_H^* \in \mathbb{R}^{h \times h}$.

Since X_H is unobserved, we only see observations from the marginal distribution of X_O . A simple calculation yields

$$(1) \quad X_O \sim \mathcal{N} \left\{ 0, \left(K_O^* - K_{HO}^{*T} K_H^{*-1} K_{HO}^* \right)^{-1} \right\}.$$

Setting $L^* := K_{HO}^{*T} K_H^{*-1} K_{HO}^*$, we have that L^* summarises the effect of the hidden variables on the observed ones. In practice, only samples drawn from $\mathcal{N}(0, (K_O^* - L^*)^{-1})$ are available and the data at our disposal is summarised by

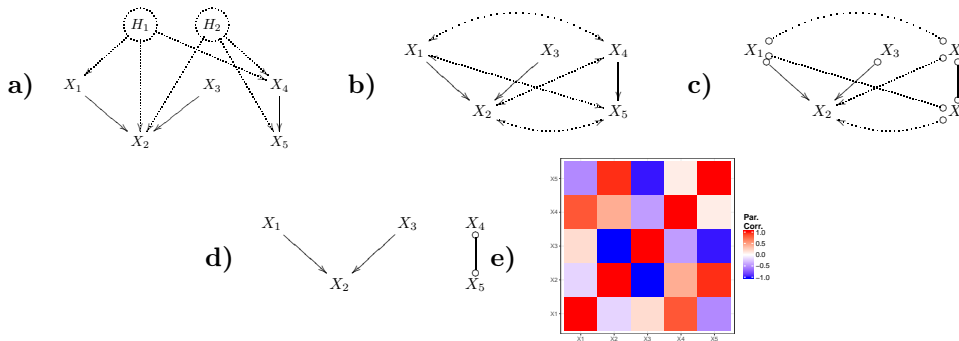


FIGURE 1. An example of a DAG, \mathcal{G}^* , with two hidden variables (H_1, H_2) and the corresponding constructions. **a)** \mathcal{G}^* . **b)** The MAG associated with \mathcal{G}^* when H_1, H_2 are marginalised out. **c)** The PAG representing the Markov equivalence class of the MAG. **d)** The CPDAG \mathcal{C}_O^* associated with the observed part of \mathcal{G}^* . **e)** The matrix L^* . It has no zero entries.

their sample covariance matrix $\hat{\Sigma}_O^n$. By assumption b), there exists a DAG, \mathcal{G}_O^* say, that is a perfect map of the distribution $\mathcal{N}(0, K_O^{*-1})$. The CPDAG of \mathcal{G}_O^* is denoted by \mathcal{C}_O^* . Our goal is to recover \mathcal{C}_O^* . In a causal framework, this also enables the use of the (joint-)IDA algorithm [28, 32]. Beyond its capacity to recover \mathcal{C}_O^* , an ideal procedure should also be well-behaved in high-dimensional settings and tractable at scale.

In Figure 1 a) we give an example of a DAG with two influential hidden variables. In such a scenario, we see that the MAG and PAG (Fig. 1 b), c)) are dense and the PAG contains many uninformative circle edgemarks. For comparison, Figure 1 d) depicts our target object \mathcal{C}_O^* which is sparse and contains more informative edge marks. Figure 1 e) shows the corresponding L^* matrix for some choice of coefficients in \mathcal{G}^* . L^* is a dense, rank-2 matrix.

2.3. Suggested Estimator. The presence of hidden variables represents a substantial complication since X_O follows a normal distribution with an inverse covariance matrix $(K_O^* - L^*)$ which is the sum of two matrices. The contribution of the observed and the hidden variables is split: K_O^* is the precision matrix induced by \mathcal{G}_O^* , while L^* summarises the effect of the hidden variables on the observed ones. Since our goal is to infer \mathcal{C}_O^* , our strategy is to first tease apart the summands in order to learn K_O^* , and then to rely on this estimate to infer \mathcal{C}_O^* under the assumption that there are no confounders.

Inferring the components of $K_O^* - L^*$ from samples drawn according to (1) is a challenging problem because it is fundamentally misspecified: an infinity of pairs (\hat{K}_O, \hat{L}) can achieve the maximum value of the likelihood. Remarkably, [6] showed that it is sometimes possible to uniquely decompose $K_O^* - L^*$ into its summands. Loosely speaking, this is the case when K_O^* is sparse and there are relatively few hidden variables with an effect spread over most of the observed variables (this is detailed further in Section 3). Since $L^* = K_{HO}^{*T} K_H^* K_{HO}^*$, constraining the number of hidden variables amounts to requiring that L^* be low-rank. The ℓ_1 and

nuclear norms being convex relaxations for the ℓ_0 -norm and the rank respectively, [6] suggest regularising the maximum-likelihood estimator with these norms so as to encourage the learning of a sparse \hat{K}_O and a low-rank \hat{L} . An estimate (\hat{K}_O, \hat{L}) of (K_O^*, L^*) is obtained as the minimiser of

$$(2) \quad \arg \min_{K_O - L \succ 0, L \succeq 0} -\ell(K_O - L; \Sigma_O^n) + \eta_n(\gamma \|K_O\|_1 + \|L\|_*),$$

where $\ell(K; \Sigma_O^n) = -\text{Trace}(K \Sigma_O^n) + \log \det K$ and $\eta_n, \gamma > 0$. Here, the notations $K_O - L \succ 0$ and $L \succeq 0$ indicate that $K_O - L$ and L are restricted to the space of positive definite and positive semi-definite matrices, respectively. Moreover $\|L\|_*$ is the nuclear norm of L (*i.e.* the sum of its singular values); $\|K_O\|_1$ is the ℓ_1 -norm of K_O (*i.e.* the sum of its entries' magnitudes). Under suitable regularity conditions, this estimator is consistent. Moreover, (2) is jointly convex in its parameters and can be efficiently minimised even when p is in the thousands [26]. We call this estimator the ‘‘low-rank plus sparse’’ estimator (LRpS) and we write $LRpS(\eta_n, \gamma; \hat{A})$ for the program which applies (2) to a covariance matrix \hat{A} , with tuning parameters η_n, γ and outputs a pair of matrices (\hat{K}_O, \hat{L}) .

Provided the conditions for consistency of LRpS are met, an algorithm which assumes causal sufficiency can be readily applied to the estimated covariance matrix \hat{K}_O^{-1} . For this second stage, we suggest using the GES algorithm with an ℓ_0 -regularised log-likelihood score [7]. Let us write $GES(\lambda_n, \hat{A})$ for the program which applies GES to a covariance matrix \hat{A} with tuning parameter λ_n and outputs a CPDAG \hat{C}_O . The suggested estimator, called $LRpS+GES$ henceforth, can be summarised as in Algorithm 2.1.

Algorithm 2.1 Description of the LRpS+GES estimator

Input: Sample covariance matrix $\hat{\Sigma}_O^n$, tuning parameters: $\eta_n > 0$, $\gamma > 0$, $\lambda_n > 0$.

Output: \hat{C}_O , an estimate of the true CPDAG C_O^* .

1 - $(\hat{K}_O, \hat{L}) \leftarrow LRpS(\eta_n, \gamma; \hat{\Sigma}_O^n)$.

2 - $\hat{C}_O \leftarrow GES(\lambda_n; \hat{K}_O^{-1})$.

At a practical level, the fact there are three tuning parameters might be a legitimate concern. We suggest first selecting the tuning parameters of $LRpS$ – η_n, γ – using cross-validation or the (extended) BIC [14] and then choosing λ_n , so that there is no need to scout a 3-dimensional grid. Moreover, we will see that both theoretical and empirical results support the idea that LRpS is not very sensitive to the value of γ : trying only a few values (*i.e.* five or so) of this tuning parameter is enough for most applications. More practical details are given later.

2.4. Previous Work. Over the past two decades, significant advances have been made on the problem of estimating DAGs from observational data. This is a task which is known to be very challenging, especially in the high-dimensional setting. For example, the space of DAGs is non-convex and its size increases super-exponentially with the dimension of the problem [38]. Structure learning algorithms fall into three categories that we review here. Since there are many approaches in each of these categories we refer the reader to [19], [12], [22] for a more detailed overview and simulation studies.

Score based approaches assign a score to each structure and aim to identify the one (or ones) that maximises a scoring function. Usually, the scoring criterion measures the quality of a candidate structure based on the data. Due to its theoretical properties and its performance on real and simulated datasets, we give special attention to the Greedy Equivalence Search (GES) algorithm of [7]. GES is a greedy algorithm which searches for the CPDAG that maximises the ℓ_0 -penalised log-likelihood score over the space of CPDAGs. It proceeds with a forward phase in which single edge additions are carried out sequentially so as to yield the largest possible increase of the score criterion, until no addition can improve the score further. The algorithm then starts with the output of the forward phase and uses best single edge deletions until the score can no longer be improved. In spite of being a greedy algorithm, GES is consistent not only in the classical sense (“fixed p , increasing n ”) [7] but also in certain sparse high-dimensional regimes [39, 31].

Constraint based algorithms learn graphical models by performing conditional independence tests. The PC-algorithm is a popular approach that falls in this category [40]. Under suitable conditions, it is consistent for CPDAG recovery, even in the high-dimensional regime [23, 20, 9]. When there are hidden variables and/or selection bias, the counterpart of the PC-algorithm is the Fast Causal Inference (FCI) algorithm [41] whose output is a partial ancestral graph [40, 37]. While consistent in sparse high-dimensional settings [10], FCI is not fast enough to be applied to large graphs. This limitation prompted the development of methods such as the *Really Fast Causal Inference* (RFCI) algorithm and FCI+ [10, 8]. A strength of FCI-type algorithms is that the hidden structure can be arbitrarily complicated, since no assumptions are made about selection bias and hidden variables.

Hybrid algorithms combine constraint-based and score-based methods. For example, the (Max-Min Hill-Climbing) MMHC algorithm first learns the skeleton using a local discovery algorithm and then orients the edges via a greedy hill-climbing procedure [43]. The NSDIST approach suggested in [19] also outputs a DAG in two-stages. In the first stage, the adaptive-lasso [47] is used to perform neighbourhood selection. For the second stage, [19] suggest a novel greedy algorithm which searches the space of DAGs whose neighbourhoods agree with the output of the first stage. Finally, the adaptively restricted GES of [31] is a hybrid approach which modifies the forward phase of GES by adaptively restricting the search space. They show that this approach is consistent in some sparse high-dimensional regimes, and much faster than GES.

The type of confounding we consider in this paper is ubiquitous in genomics applications, which is why the problem of estimating and removing this kind of unwanted variation has been well-studied [25, 16, 30]. A simple approach consists in estimating the first few principal components of the data and to regress them out before conducting any analysis. More sophisticated, general purpose algorithms have also been developed. PEER, for example, is a Bayesian approach which aims at inferring “hidden determinants and their effects from gene expression profiles by using factor analysis methods” [42]. It was recently used by the GTEx consortium in order to remove confounding from their datasets [1].

3. THEORETICAL RESULTS

The high-dimensional behaviour of the Low-Rank plus Sparse decomposition (LRpS henceforth) and the GES algorithm has been studied in the literature [6,

31]. We rely on this body of work to derive the high-dimensional consistency of LRpS+GES.

We consider an asymptotic scenario where both the dimension of the problem and the sample size are allowed to grow simultaneously, meaning that p and h are now functions of n . We write p_n and h_n to make this dependence explicit. Likewise, we write $X_n = (X_{nO}^T, X_{nH}^T)^T \in \mathbb{R}^{p_n+h_n}$ for the random vectors being modelled, where $X_{nO}^T = (X_{n1}, \dots, X_{np_n})^T$. We also write K_{nO}^* , L_n^* and C_{nO}^* to make it clear that the nominal parameters and the estimates obtained from Algorithm 2.1 (\hat{K}_{nO} , \hat{L}_n , \hat{C}_{nO}) are indexed by n . We let $\rho_{nij|U}^*$ be the true partial correlation between X_{ni} and X_{nj} given $\{X_{nl} : l \in U\}$, for $i, j \in \{1, \dots, p_n\}$ and $U \subseteq \{1, \dots, p_n\} \setminus \{i, j\}$. The sample partial correlation $\hat{\rho}_{nij|U}$ is defined similarly. These quantities can be computed from K_{nO}^{*-1} and \hat{K}_{nO}^{-1} . For any matrix M , we denote by $\text{degree}(M)$ the maximum number of non-zero entries in any row or column of M . If \mathcal{G} is a partially directed graph with adjacency matrix M , we define its degree $\text{degree}(\mathcal{G}) := \text{degree}(M)$. Finally, for any matrix M , let $\|M\|_2$ be the spectral norm of M , *i.e.* its largest singular value, and let $\|M\|_\infty$ be its largest entry in magnitude, *i.e.* $\|M\|_\infty = \max_{i,j} |M_{ij}|$.

We prove the following result in Appendix A.

Theorem 3.1. *Assume (A1) - (A6) given below. Then, there exists a sequence $\lambda_n \xrightarrow{n \rightarrow \infty} 0$ such that $\mathbb{P}(\hat{C}_{nO} = C_{nO}^*) \xrightarrow{n \rightarrow \infty} 1$.*

Assumptions (A1) - (A6) are as follows:

- (A1): (Consistency of LRpS) The conditions for the algebraic consistency of LRpS are satisfied (see Theorem 4.1 of [6]). In particular, it is required that both observed and hidden variables be jointly normal.
- (A2): (High-dimensional setting) $p_n = \mathcal{O}(n^{1-a})$, for some $0 < a \leq 1$.
- (A3): (Sparsity condition) Let $q_n = \text{degree}(C_{nO}^*)$ and $q'_n = \text{degree}(K_{nO}^*)$, so that $q_n \leq q'_n$. We assume that $q'_n = \mathcal{O}(\log(n)^b)$, for some $0 \leq b \leq \infty$.
- (A4): (Bounds on the growth of the oracle versions) The maximum degree in the output of the forward phase of every δ_n -optimal oracle version of GES is bounded by $K_n q_n = \mathcal{O}(n^{1-f})$, for some sequence $\delta_n^{-1} = \mathcal{O}(n^{d_1})$ such that $0 < f \leq 1$ and $0 \leq d_1 < f/2$, and where q_n is given by (A3).
- (A5): (Bounds on partial correlations) The partial correlations $\rho_{nij|U}^*$ satisfy the following upper and lower bound for all n and $U \subseteq \{1, \dots, p_n\} \setminus \{i, j\}$ such that $|U| \leq K_n q_n$:

$$\sup_{i \neq j, U} |\rho_{nij|U}^*| \leq M < 1, \text{ and } \inf_{i, j, U} \{|\rho_{nij|U}^*| : \rho_{nij|U}^* \neq 0\} \geq c_n,$$

with $c_n^{-1} = \mathcal{O}(n^{d_2})$ for some $0 \leq d_2 < f/2$ where f is as in (A4).

- (A6): $\|K_{nO}^{*-1}\|_2 < C_4$ and $\|K_{nO}^*\|_\infty < C_5$, for some $C_4, C_5 \geq 0$.

In the previous section, it was mentioned that the LRpS estimator is consistent when K_{nO}^* is sparse and L_n^* is low-rank. Assumption (A1) contains more precise requirements for the problem to be identified. One of the conditions for identifiability is expressed as $\xi(L_n^*)\mu(K_{nO}^*) \leq \frac{1}{6}C^2$, for some constant C which depends on the Fisher information matrix. Here, $\xi(L_n^*)$ is a property of L_n^* such that a small value of $\xi(L_n^*)$ guarantees that no single hidden variable will have an effect on only a small number of the observed variables. It is related to the concept of

incoherence, which is easily calculated and satisfies $\text{inc}(M) \leq \xi(M) \leq 2\text{inc}(M)$, for any matrix M [5, 6]. On the other hand, $\mu(K_{nO}^*)$ quantifies the diffusivity of K_{nO}^* 's spectrum. Matrices that have a small μ have few non-zero entries per row/column. Thus, (A1) entails that there must be few hidden variables acting on many observed ones and that K_{nO}^* must have sparse rows/columns. Assumption (A1) also requires that the tuning parameter γ be chosen within the range $\left[\frac{3\xi(L_n^*)}{C}, \frac{C}{2\mu(K_{nO}^*)}\right]$, thus supporting our observation that LRpS is not very sensitive to the value of this tuning parameter in practice.

An important feature of Theorem 3.1 is that the degrees of the true CPDAG and K_{nO}^* are allowed to grow logarithmically with the sample size n . When coupled with (A1), this assumption on the growth rate of q'_n imposes restrictions on the number of hidden variables h_n , albeit not explicitly. Indeed, it can be shown that for the condition $\xi(L_n^*)\mu(K_{nO}^*) \leq \frac{1}{6}C^2$ to hold with high probability, h_n has to be of the form $h_n = \mathcal{O}\left(\frac{p_n}{\log(p_n)^{2d}}\right)$ (under some assumptions about the distribution from which L_n^* is sampled) [6]. Thus, the degree of C_{nO}^* and the number of hidden variables are allowed to grow simultaneously with the sample size.

We note that [31] proved high-dimensional consistency of GES under weaker versions of (A2) and (A3). Namely, GES allows $p_n = \mathcal{O}(n^a)$ for some $0 \leq a < \infty$ and $q_n = \mathcal{O}(n^{1-b})$ for some $0 < b \leq 1$. Second, assumption (A1) includes stringent conditions on the value of the smallest eigenvalue of L_n^* as well as a form of ‘‘generalised irrepresentability condition’’ similar to the irrepresentability condition introduced in [35] in the context of ℓ_1 -regularised maximum likelihood estimation. In the next section, we illustrate the performances of LRpS+GES on simulated data both when our assumptions hold and when they are grossly violated. Just like its ℓ_1 -regularised counterpart (the graphical lasso), we find that LRpS performs well in many more settings than suggested by theory. In the case of the graphical lasso, this is explained by the so-called ‘‘screening property’’. To the best of our knowledge, no such theoretical results exist for LRpS.

4. PERFORMANCES ON SIMULATED DATA

4.1. CPDAG Structure Recovery. Throughout, we generate DAGs with $p + h$ nodes, and set $p = 50$ – a value which does not depend on the sample size n^2 . Thus, our data is generated according to linear structural equation models of the form

$$X \leftarrow \begin{pmatrix} B_O^* & B_{OH}^* \\ 0 & B_H^* \end{pmatrix} X + \epsilon,$$

where $B_O^* \in \mathbb{R}^{p \times p}$, $B_{OH}^* \in \mathbb{R}^{p \times h}$ and $B_H^* \in \mathbb{R}^{h \times h}$ are matrices encoding the structure and effect sizes of the DAGs and $\epsilon \sim \mathcal{N}(0, \Lambda)$ [4]. Furthermore, B_O^* and B_H^* are strictly upper-triangular matrices and $\Lambda \in \mathbb{R}^{(p+h) \times (p+h)}$ is a diagonal matrix. The DAGs over the observed variables (\mathcal{G}_O^*) are random DAGs with an expected sparsity of 5%, which corresponds to an average degree of about 2.5 and an average maximum degree of about 6.3. The h hidden variables remain independent, but each of them has directed edges towards a random $f\%$ of the observed variables. All edge weights – *i.e.* the non-zero entries of the B^* matrices – are drawn uniformly at random from $[-1, -0.3] \cup [0.3, 1]$. Residual variances – *i.e.* the diagonal entries of Λ – follow a uniform distribution over $[1/2, 3/2]$.

²The code for our simulations and applications is made available with this paper.

In this section, we compare methods based on the precision-recall curves obtained by varying the tuning parameter for the last stage of the structure learning methods. The tuning parameters of the first stages (when applicable) are selected as described below. The following methods are applied to the data:

- GES [7]:** implemented in the `pcalg` package [24].
- NSDIST [19]:** we used the code made available with the original article. For the tuning parameters of the first stage (called λ_0 and γ in [19]), we used the values suggested in [19].
- PCA*+GES:** the top k principal components are first estimated from the data matrix and regressed out. GES is then applied to the residuals. The number of principal components is chosen with *perfect knowledge* (hence the * in the name) so as to maximise the average precision.
- PEER*+GES [42]:** similar to PCA*+GES, the first stage is replaced with PEER. Here again, the number of latent factors is selected so as to maximise average precision, hence the * in the name.
- LRpS+GES:** the suggested approach described in Algorithm 2.1. The tuning parameters η_n, γ for LRpS are chosen by cross-validation with $\gamma \in \{0.05, 0.1, 0.15, 0.2, 0.3, 0.5, 0.7\}$.

In our first set of simulations, we investigate the effect of the sample size n and the number of hidden variables h on CPDAG recovery. We set $n \in \{50, 500, 1000\}$ and $h \in \{0, 5, 10\}$, but fix f to 70. For each of the nine possible (n, h) pairs, we generate 50 distinct DAGs and draw n samples from each of them, for a total of 450 datasets. This is a setting which is favourable to our approach since the hidden variables impact a large fraction (70%) of the observed ones.

In Figure 2 **a**) we assess the performances of the methods in terms of skeleton recovery by plotting average precision/recall curves. Precision is calculated as the fraction of correct edges among the retrieved edges; recall is computed as the number of correctly retrieved edges divided by the total number of edges in the true CPDAG. Since each of the 9 designs is repeated 50 times, we report average precisions at fixed recalls of $\{0.01, 0.02, \dots, 1\}$. In the appendix, similar curves are plotted for directed edges. When there is no confounding (leftmost column), all methods are known to be consistent for skeleton recovery and offer comparable performances. As soon as $h > 0$, GES is outperformed. Unsurprisingly, when n and p are of the same order of magnitude, PCA does not perform as well as a Bayesian approach like PEER. When there are only a few confounders ($h = 5$, middle column) they both perform significantly better than GES. When it comes to skeleton recovery, LRpS+GES is always at least as good as the other methods. When there is confounding, it is significantly better because it is the only method which explicitly models hidden variables. This is true even though the tuning parameters η_n and γ were chosen with cross-validation. We also see that when $h > 0$, LRpS+GES is the only method whose performance improves with increasing sample size.

In our second set of simulations, we draw from a more diverse set of hidden structures. We set $n = 1000$ but draw h and f uniformly at random from $[5, 30]$ and $[15, 70]$ respectively. We generate 500 datasets according to this scheme. In order to quantify the departure of L^* from our assumptions we compute $inc(L^*)$, the incoherence of L^* , for each of the 500 datasets (the distribution of $inc(L^*)$ along with figures showing the effect of h are shown in the appendix). In this

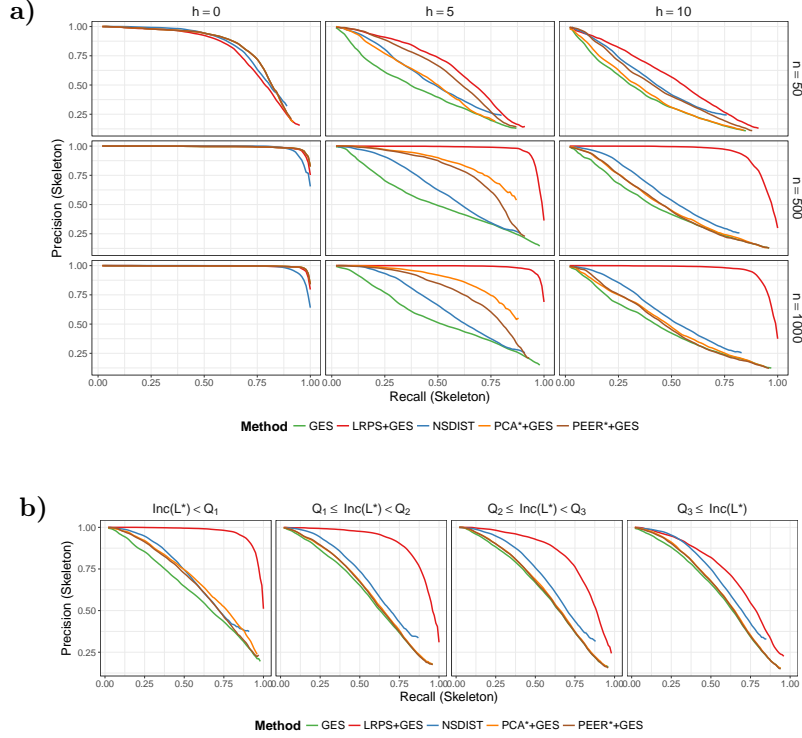


FIGURE 2. Average precisions at fixed recalls of $\{0.01, 0.02, \dots, 1\}$ for skeleton recovery. There are $p = 50$ observed variables. **a)** Effect of the number of hidden variables (h) and sample size (n), when $f = 70$ and each of the 9 designs is repeated 50 times. **b)** Effect of the incoherence of the latent structure $\text{inc}(L^*)$. The 500 random datasets are binned according to the quartiles of $\text{inc}(L^*)$'s distribution ($Q_1 - Q_4$).

second scenario, many datasets explicitly violate our assumptions since there are many hidden variables acting in a sparse fashion.

In Figure 2 **b)**, we plot average precision/recall curves for this second simulation design. The datasets are divided into four bins based on the quartiles of $\text{inc}(L^*)$'s distribution (noted $Q_1 - Q_4$), so that the leftmost panel corresponds to the 125 datasets for which it is easiest to estimate L^* . Doing so indicates how our approach is expected to behave in the most adverse scenarios. As can be seen from this figure, LRPS+GES performs at least as well as other approaches in terms of skeleton recovery. In most cases, it performs better.

4.2. Total Causal Effect Estimation. Under the additional assumption that \mathcal{G}_O^* – which is a perfect map of the distribution $\mathcal{N}(0, K_O^{*-1})$ – is the causal DAG, the Markov equivalence class encoded by \mathcal{C}_O^* contains the causal DAG. For any given pair of distinct nodes (X_i, X_j) , we can therefore estimate the total causal effect

of X_i on X_j for all DAGs in the Markov equivalence class. Since one of these DAGs is the true causal DAG, this yields a list of possible total causal effects which includes the true total causal effect. The IDA approach makes it possible to generate such lists efficiently without enumerating all DAGs in the Markov equivalence class [28, 27]. The original IDA method described in [28] uses the PC algorithm in order to first estimate a CPDAG, and then computes sets of possible total causal effects using the sample covariance matrix and the output of the first stage. However, it is possible to replace this first step by any other algorithm which estimates a CPDAG. Likewise, any estimator of Σ_O^* can replace $\hat{\Sigma}_O^n$.

Since LRPS+GES outputs a CPDAG, we can assess its ability to estimate total causal effects by using it in the first stage of IDA. Thus, lists of possible causal effects are generated using the estimated CPDAG \hat{C}_O and the covariance matrix \hat{K}_O^{-1} . We denote this method by (LRPS+GES),IDA. For all pairs $(i, j) \in \{1, \dots, p\}^2$, $i \neq j$, we compute the set S_{ij} of possible total causal effects of X_i on X_j . Pairs of variables (X_i, X_j) are then ranked according to $\min(\{|s| : s \in S_{ij}\})$. This ranking is compared to the true total causal effects using the precision and recall metrics, *e.g.* “precision at rank k ” would be the number of pairs (X_i, X_j) that are in the top k pairs and have a non-zero total causal effect in the true DAG, divided by k .

In this section, we select a single DAG, PAG or CPDAG along the regularisation paths in order to apply IDA or LV-IDA. Thus, we pick a value of the tuning parameters for both the first and second stages. This is in contrast with the previous section where only the tuning parameters of the first stages (when applicable) were selected, while we reported precision-recall curves for the whole regularisation paths of the second stages. We consider the following methods, where the first stage tuning parameters are selected as before (when applicable):

GES,IDA: the CPDAG is estimated using GES. The tuning parameter λ_n is chosen with the BIC. IDA is applied with the resulting CPDAG and the sample covariance matrix $\hat{\Sigma}_O^n$.

NSDIST,IDA: the DAG is estimated using NSDIST and converted to a CPDAG. The tuning parameter for the second stage (λ , with the notations of [19]) is chosen using the BIC. IDA is applied with the resulting CPDAG and the sample covariance matrix $\hat{\Sigma}_O^n$.

(PCA*+GES*),IDA: : the top k principal components are first estimated from the data and regressed out. The CPDAG is estimated using GES on the residuals. The tuning parameter λ_n is chosen with perfect knowledge so as to maximise the average precision (in terms of causal effect recovery). IDA is applied with the resulting CPDAG and the covariance matrix of the residuals.

(LRpS+GES),IDA: the CPDAG is estimated using LRpS+GES. The tuning parameter of the second stage λ_n is chosen with the BIC. IDA is applied with the resulting CPDAG and the covariance matrix \hat{K}_O^{-1} .

RFCI, LV-IDA [10, 29]: the PAG is estimated with RFCI. The significance level α for RFCI is given by $\alpha = \frac{0.5}{\sqrt{n}}$ ³. LV-IDA is applied to the resulting PAG and the sample covariance matrix $\hat{\Sigma}_O^n$. Whenever LV-IDA outputs an

³In a number of cases, the LV-IDA algorithm, when applied to a single dataset, was still running after a few days of computation. Given that we simulated data from hundreds of datasets, we could not experiment with many values of α .

NA, the corresponding pair is not counted, *i.e.* it is neither a true positive nor false positive.

RANDOM,IDA: one hundred random DAGs are generated from the same model as was used in the simulation. Total causal effects are then estimated based on the resulting CPDAG and the sample covariance matrix $\hat{\Sigma}_O^n$. We report the interval spanned by the 2.5-97.5 percentiles of the distribution of precisions at fixed recalls.

EMPTY, IDA: Causal effects are computed without adjustment, which is equivalent to applying the `ida` function of the `pcaIlg` package to an empty graph and the sample covariance matrix.

With respect to total causal effect estimation, we found (PEER*+GES*),IDA and (PCA* + GES*),IDA to be nearly undistinguishable, which is why PEER is not reported here. Moreover, note that since we are reporting results for the GES,IDA approach, we are not considering the “PC,IDA” method. Indeed, GES has been shown to have good finite sample performance, and recent high-dimensional consistency guarantees have been given in [31].

We consider the same simulation designs as in the previous section. Figure 3 **a**) displays the results obtained in the first setting, the one where hidden variables are influential. Unlike in Figure 2, the orientation of the directed edges matters. When the sample size is relatively small ($n = 50$), there appear to be little to gain from using (CP)DAG estimation methods – the EMPTY approach is competitive. As soon as the sample size increases and $h > 0$, there is a clear benefit in using LRpS+GES. When $h = 0$, LRpS+GES is outperformed but its performances remain comparable to those of GES. Since it is designed to handle hidden variables, the behaviour of RFCI,LV-IDA might come as a surprise. First, we see that when there is no confounding, RFCI,LV-IDA is capable of achieving a higher precision than any other method. This is consistent with previous findings indicating that LV-IDA is conservative but capable of recovering a small but high-quality set of total causal effects [29]. When $h > 0$, the set of models we simulate from is particularly challenging for methods relying on MAGs since nearly all pairs of observed variables are confounded. It is therefore not surprising to see RFCI,LV-IDA being outperformed.

As can be seen from Figure 3 **b**), LRpS+GES performs at least as well other approaches and, in most cases, it performs better. As pointed out above, it is in the most challenging scenarios, when confounders act in a sparse fashion (rightmost panel), that RFCI,LV-IDA is the most useful. It is very conservative but is capable of achieving the highest precision.

5. APPLICATIONS

5.1. Application 1: Isoprenoid Synthesis in *Arabidopsis thaliana*. We illustrate a few properties of our approach on a dataset containing gene expression measurements taken in *Arabidopsis thaliana* under $n = 118$ experimental conditions [45]. [45] gave particular attention to the genes involved in isoprenoid synthesis. In *Arabidopsis thaliana*, two pathways, located in distinct organs, are responsible for isoprenoid synthesis: the mevalonate pathway (MVA) and the non-mevalonate pathway (MEP). We downloaded the data made available in the supplementary materials of [45] and modelled the $p = 33$ genes represented in Figure 3 of [45]. They fall into three categories: genes that are part of the MVA pathway, genes that

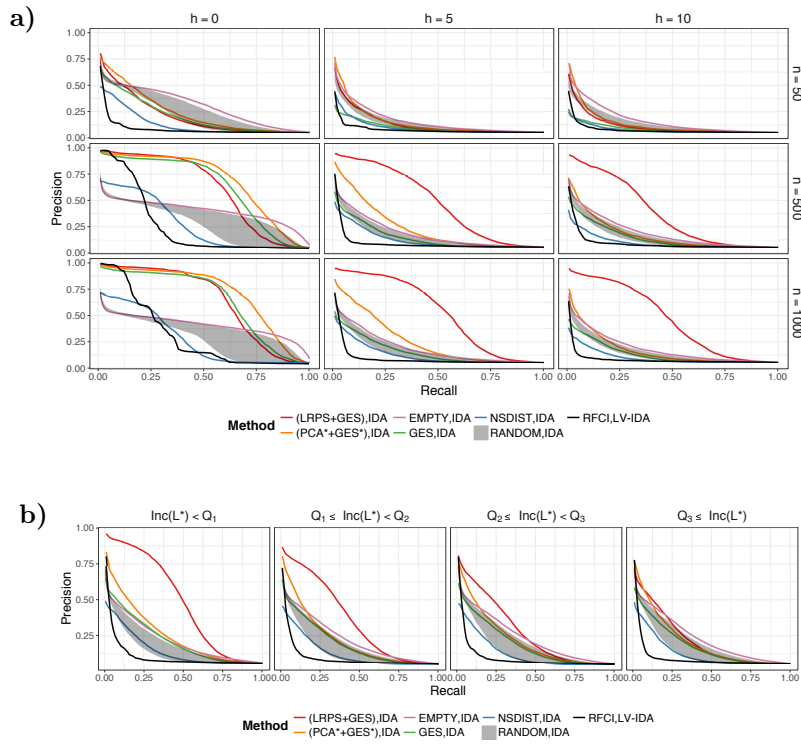


FIGURE 3. Average precisions at fixed recalls of $\{0.01, 0.02, \dots, 1\}$ for total causal effect recovery. **a)** Effect of the number of hidden variables (h) and sample size (n) when $f = 70$ and each of the 9 designs is repeated 50 times. **b)** Effect of the incoherence of the latent structure $inc(L^*)$. The 500 random datasets are binned according to the quartiles of $inc(L^*)$'s distribution ($Q_1 - Q_4$).

are in the MEP pathway and mitochondrial genes. For illustration, Figure 4 **a)** shows the adjacency matrix of the metabolic pathways. This is a graph in which nodes are genes and edges are chemical reactions between gene products. This graph, while related to the regulatory network we aim to estimate, is very different from it: in general, both the structure and the direction of the edges differ.

We fitted LRpS to our data and selected the tuning parameters η_n and γ with five-fold cross-validation. The estimated low-rank matrix \hat{L} had two non-zero eigenvalues, with ratio $\frac{\hat{\sigma}_1}{\hat{\sigma}_2} = 347$. Hence, only the first eigenvector was retained. In order to see whether we could interpret the hidden variables estimated by LRpS, we looked at the loadings of the genes in the first eigenvector of \hat{L} . Figure 4 **b)** shows the distribution of the loadings per pathway and suggests that the main source of variation in the data is given by these pathways, which are sometimes unknown in less studied organisms. This shows that in some cases, we can account for hidden variables, but also interpret them. By applying GES to \hat{K}_O^{-1} – the sparse output

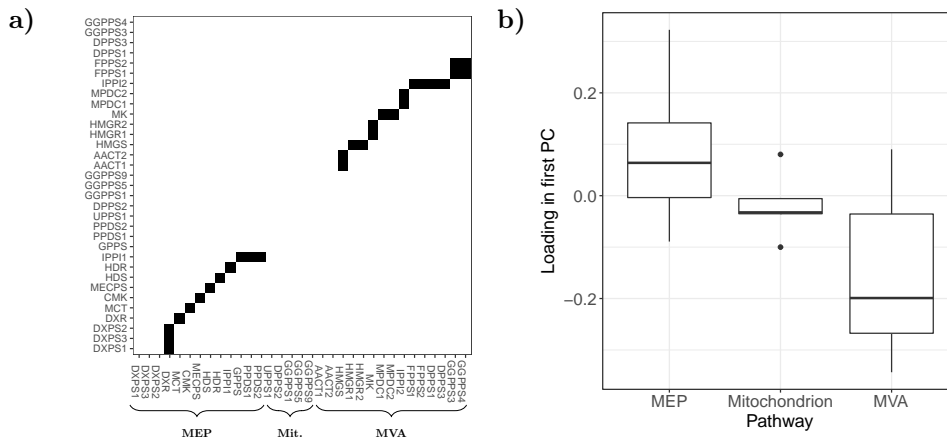


FIGURE 4. **a)** Directed graph induced by the MVA and MEP metabolic pathways, as shown in Figure 3 of [45]. A non-zero entry (i,j) indicates a directed edge $i \rightarrow j$. **b)** Per pathway distribution of the entries of \hat{L} 's first eigenvector.

of LRpS – we are therefore modelling a regulatory network conditionally on those pathways, without having to provide further information.

In Figures 5 **a)** and **b)**, we show the adjacency matrices of the CPDAGs obtained by running GES and LRpS+GES using the BIC score for GES. Figure 5 **c)** shows the adjacency matrix of the PAG obtained by RFCI, with $\alpha = \frac{0.5}{\sqrt{n}}$ as before. In Figures 5 **d)**, **e)**, the matrices of total causal effects computed from GES,IDA and (LRpS+GES),IDA are plotted, where IDA is used as in our simulations. In Figure 5 **f)**, the output of LV-IDA is plotted, with NAs marked in red. The graphs and total causal effects obtained from other methods (NSDIST,IDA, etc...) are plotted in the appendix. Figure 5 illustrates the tendency of LV-IDA to produce very conservative estimates of the causal effects, with many pairs being either zero or NA. On the other extreme, the causal effects of GES are stronger than those of LRpS+GES. In particular, LRpS+GES does not find any strong causal relationship between mitochondrial genes and any other genes, as indicated by the “white cross” in the middle of the matrix plotted in Figure 5 **e)**. Both GES and LRpS+GES support the hypothesis of cross-talk from the MEP to the MVA pathway.

The metabolic pathways of *Arabidopsis thaliana* have been studied in detail but, to the best of our knowledge, no reliable ground-truth is available for its directed regulatory network. For that reason, it is difficult to assess the quality of the estimated CPDAGs or matrices of total causal effects. Nonetheless, by applying LRpS+GES to this dataset, we were able to show that it is sometimes possible to interpret the latent factors inferred by our approach. Moreover, this type of confounding is not specific to this particular dataset, but is expected to occur in most gene expression datasets, possibly in organisms for which no pathway information is available. This application also gave us the opportunity to compare LV-IDA to other IDA-based methods on a real dataset.

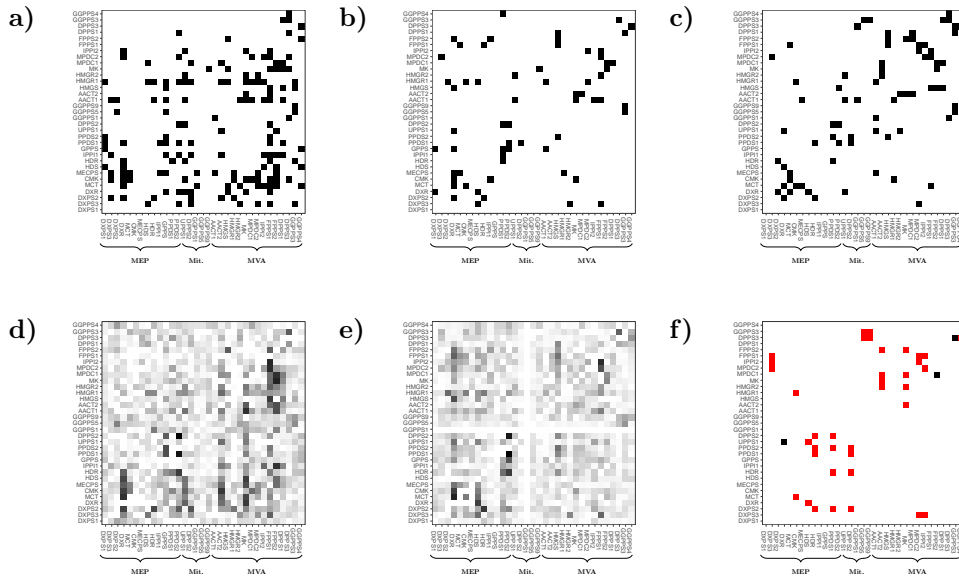


FIGURE 5. Estimates obtained by applying GES, LRpS+GES and RFCI to the data of [45]. **a)** Adjacency matrix of the CPDAG estimated by GES. **b)** As in a), but with LRpS+GES. **c)** Adjacency matrix of the PAG estimated by RFCI with $\alpha = \frac{0.5}{\sqrt{n}}$. **d)** Matrix of total causal effects for GES,IDA. **e)** As in d), but with LRpS+GES. **f)** Matrix of total causal effects for RFCI,LV-IDA. NA entries are plotted in red.

5.2. Application 2: Regulatory Network in Ovarian Cancer. We now consider the problem of identifying the targets regulated by a given set of transcription factors in a human gene expression dataset. This problem is often considered in the literature because it constitutes an example of a real-life dataset for which the existence and direction of *some* edges is known, thus making it possible to compare estimated graphs to a “partial ground-truth” [43, 19]. Briefly, a *transcription factor* is a protein which regulates the mRNA expression of a gene by binding to a specific DNA sequence near its promoting region. Some families of transcription factors have been studied in detail, and publicly available databases such as TRRUST provide lists of transcription factors along with the genes – called *targets* – they regulate [18]. transcription factors play a crucial in role in cancer development, which is why it is believed that intervening on the expression of such genes could alter the course of some cancers [11].

In this application, we follow closely the steps described in Section 5.1 of [19] where ovarian adenocarcinomas are studied. We used the RNA-Seq data available from the National Cancer Institute (portal.gdc.cancer.gov/) and log-transformed the gene expression levels. There is a consensus about how important some transcription factor families are for cancer development [11, 36]. We therefore selected

the transcription factors belonging to those families⁴. Following [19], we also extracted the genes that are known to have direct interactions with these transcription factors according to NetBox⁵, “a software tool for performing network analysis on human interaction networks which is pre-loaded with networks derived from four curated data sources, including the Human Protein Reference Database (HPRD), Reactome, NCI-Nature Pathway Interaction (PID) Database, and the MSKCC Cancer Cell Map”. The resulting dataset contained $p = 501$ genes and $n = 247$ samples.

To construct a reference network to which we can compare our estimates, we used the output of NetBox. NetBox outputs a list of known (unoriented) interactions between some of the 501 selected genes. Unfortunately, nothing indicates whether those interactions are causal; in general it is not because two genes interact in NetBox that intervening on the expression levels of one of the genes will induce a change in the expression level of the other. However, thanks to our knowledge of transcription factors, we do know that whenever there is an interaction between a transcription factor and a non-transcription factor, then it is likely to be causal and directed from the transcription factor to its target. Moreover, transcription factors are tissue specific, meaning that we can only expect a subset of the interactions to be active in any given cell-type [13]. These observations allow us to build three reference networks: *a*) an undirected graph in which there is an edge between A and B whenever they are said to interact according to NetBox (this is Network A); *b*) a “causal” undirected graph in which only edges between transcription factors and their targets have been retained (Network B); *c*) a causal directed graph in which the edges of Network B have been ordered from transcription factors to their targets (Network C).

In this application, the number of variables ($p = 501$) is rather large compared to the sample size ($n = 247$). We therefore selected the tuning parameters of LRpS (η_m, γ) using the Extended BIC instead of cross-validation [14].

In Figure 6 we compare the output of various methods (GES, LRpS+GES, NSDIST, PCA*+GES, PEER*+GES) to reference networks A, B and C in terms of True and False Positive Rates (TPR, FPR). For Network C, we follow again [19]: an undirected edge in a CPDAG is counted as half a true positive and half a false negative. In grey, we plot the range spanned by the 2.5 and 97.5 percentiles of our null distribution. It was computed by first picking 100 random ordering of the variables and, starting from a complete DAG, removing random edges one after the other until there are no edges left. After each removal, we computed the performance metrics of the DAG with respect to all reference networks, thus generating 100 random regularisation paths for each of the plots.

Figure 6 **a**) plots the Receiving Operator Curve (ROC) for Network A. All methods display comparable performances, although NSDIST and LRpS+GES appear slightly above GES. In Figure 6 **b**), we restrict ourselves to Network B, so that only transcription factor-target edges are counted. LRpS+GES is clearly above NSDIST, PCA*+GES and PEER*+GES which are themselves outperforming GES. When the direction of the edges is also taken into account (Figure 6 **c**)), LRpS+GES remains ahead of the other methods, and NSDIST beats PCA and PEER. The

⁴Namely: FOS, FOSB, JUN, JUNB, JUND, ESR1, ESR2, AR, NFKB1, NFKB2, RELA, RELB, REL, STAT1, STAT2, STAT3, STAT4, STAT5, STAT6

⁵<http://sanderlab.org/tools/netbox.html>

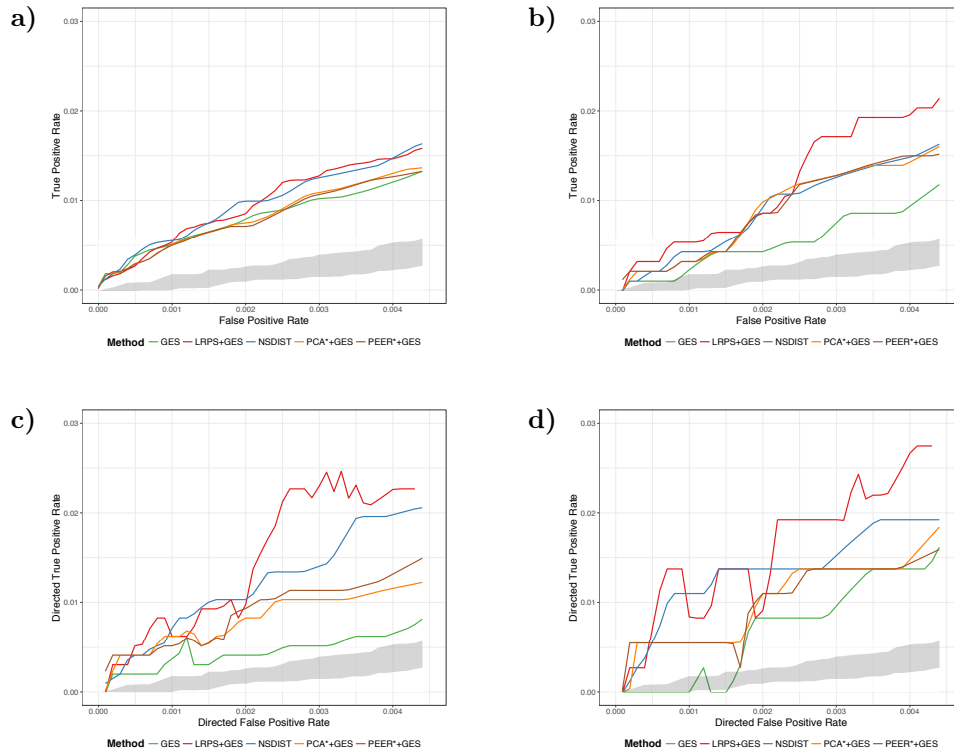


FIGURE 6. Comparison of the estimates of various methods against reference networks A, B, C and D. **a)** ROC curves comparing the skeleton of the estimates to the undirected NetBox network (Network A). **b)** Same as a), but for the causal undirected network (Network B). **c)** ROC curves comparing the estimated CPDAG (or DAG in the case of NSDIST) to the directed causal network (Network C). **d)** Same as c), but with the directed network induced by TRRUST (Network D).

difference in performance between NSDIST and GES does not come as a surprise since Figure 6 **a)** and **b)** reproduce the findings of Figures 4 **a)** and **b)** of [19].

Since NetBox is not restricted to transcription factor-target interactions, we sought to confirm the results of Figure 6 **c)** by using an independent source of validation specialised in transcriptional regulatory relationships. We used TRRUST [18] and constructed Network D by adding directed edges between transcription factors and targets according to TRRUST. In Figure 6 **d)** we plot the resulting ROC curve, which reproduces the results obtained using NetBox transcription factor-target interactions as ground truth.

6. DISCUSSION

We discussed the problem of estimating the Markov equivalence class of a DAG in the presence of hidden variables. Building on previous work by [6] and [7], we suggested a two-stage approach – termed LRpS+GES – which first removes unwanted variation using latent Gaussian graphical model selection, and then estimates a CPDAG by applying GES. We chose GES for its good empirical performance and theoretical guarantees [31], but we note that the second step can be replaced by any structure learning algorithm for DAGs that assumes causal sufficiency. Our main theoretical result states that LRpS+GES is consistent for CPDAG recovery in some sparse high-dimensional regimes. Through simulations and two applications to gene expression datasets, we showed that our approach often outperforms the state of the art, both in terms of graphical structure recovery and total causal effect estimation. Moreover, the results reported in our simulations can be achieved in practice since tuning parameter selection was performed using in-sample information only⁶.

When it comes to removing unwanted variation from biological datasets, state-of-the-art approaches usually incorporate external information into the analysis by including additional covariates (*e.g.* gender, genetic relatedness), thus also accounting for known confounders [42, 30]. Since these additional covariates are often discrete, modelling them with LRpS+GES would be a violation of our assumptions. In such a setting, it is straightforward to replace LRpS by the LSCGGM estimator suggested in [15]. LSCGGM makes it possible to perform a low rank plus sparse decomposition, conditionally on a number of arbitrarily distributed random variables. The LRpS+GES approach could therefore be replaced by the “LSCGGM+GES” estimator, which would come with similar theoretical guarantees.

The computational cost of LRpS+GES might also be a concern to the practitioner. In Algorithm 2.1 we first estimate an inverse covariance matrix \hat{K}_O . To the best of our knowledge, the fastest algorithm for this LRpS step uses the so-called alternative direction method of multipliers, with a cost of $\mathcal{O}(p^3)$ per iteration [26]. Next, \hat{K}_O must be inverted, at a cost of $\mathcal{O}(p^3)$, and then GES is run on \hat{K}_O^{-1} . For large problems, this last step can be replaced by the ARGES algorithm suggested in [31].

As detailed earlier, there exist other approaches which are capable of estimating DAG models and total causal effects in the presence of hidden variables, *i.e.* FCI-type algorithms [41, 10, 8] and LV-IDA [29]. In both our simulations and our first application, we found that such approaches are very conservative under our assumptions. However, they do outperform LRpS+GES when hidden variables act on the observed ones in a sparse fashion. As such, LRpS+GES is complementary to existing methods.

Finally, we note that the LRpS+GES estimator can be modified to tackle another widespread problem: selection bias. Reusing the notations introduced in Section 2.2, selection bias can be handled as follows. Let $X \in \mathbb{R}^{p+h}$ be a zero-mean random vector which follows a multivariate normal distribution with *covariance* matrix $\begin{pmatrix} \Sigma_O^* & \Sigma_{OH}^* \\ \Sigma_{OH}^{*T} & \Sigma_H^* \end{pmatrix}$. Let us further assume that there exists a DAG, \mathcal{G}_O^* say, which is a perfect map of the distribution $\mathcal{N}(0, \Sigma_O^*)$. Then, assuming that the variables in

⁶The code for our simulations and applications is made available with this paper.

X_H are selection variables, we only see observations from

$$X_O|X_H \sim \mathcal{N}\left(0, \Sigma_O^* - \Sigma_{OH}^* \Sigma_H^{*-1} \Sigma_{OH}^{*T}\right).$$

By the Woodbury identity, this can be rewritten in terms of the precision matrix as

$$X_O|X_H \sim \mathcal{N}\left(0, \left(\Sigma_O^{*-1} - L^*\right)^{-1}\right),$$

where L^* is a *negative semi-definite* matrix defined as

$$L^* := -\Sigma_O^{*-1} \Sigma_{OH}^* \left(\Sigma_H^* - \Sigma_{OH}^{*T} \Sigma_O^{*-1} \Sigma_{OH}^*\right)^{-1} \Sigma_{OH}^{*T} \Sigma_O^{*-1}.$$

Since Theorem 4.1 of [6] does not make any assumptions about the positive-definitiveness of L^* , the following estimator could replace LRpS in the first stage of LRpS+GES:

$$(3) \quad \arg \min_{K_O - L > 0, L \leq 0} -\ell(K_O - L; \Sigma_O^n) + \eta_n(\gamma \|K_O\|_1 + \|L\|_*),$$

where $\ell(K; \Sigma_O^n) = -\text{Trace}(K \Sigma_O^n) + \log \det K$ and $\eta_n, \gamma > 0$. This modified approach is consistent in the presence of selection variables under the similar conditions as Theorem 3.1. The only difference is in the interpretation of the condition $\xi(T)\mu(\Omega) \leq \frac{1}{6}C^2$, which would require that Σ_O^{*-1} be sparse and that there be few selection variables that are directly regulated by many of the observed variables.

REFERENCES

- [1] Aguet, F. et al. (2016) Local genetic effects on gene expression across 44 human tissues. *Tech. rep.* Available at <http://dx.doi.org/10.1101/074450>.
- [2] Ali, R. A., Richardson, T. S. and Spirtes, P. (2009) Markov equivalence for ancestral graphs. *Ann. Statist.*, **37**, 2808–2837.
- [3] Andersson, S. A., Madigan, D. and Perlman, M. D. (1997) A characterization of Markov equivalence classes for acyclic digraphs. *Ann. Statist.*, **25**, 505–541.
- [4] Bollen, K. (1989) Structural equations with latent variables.
- [5] Candès, E. J., Li, X., Ma, Y. and Wright, J. (2011) Robust principal component analysis? *J. ACM*, **58**, Art. 11.
- [6] Chandrasekaran, V., Parrilo, P. A. and Willsky, A. S. (2012) Latent variable graphical model selection via convex optimization. *Ann. Statist.*, **40**, 1935–1967.
- [7] Chickering, D. M. (2002) Learning equivalence classes of Bayesian-network structures. *J. Mach. Learn. Res.*, **2**, 445–498.
- [8] Claassen, T., Mooij, J. M. and Heskes, T. (2013) Learning sparse causal models is not NP-hard. In *Proceedings of the Twenty-Ninth Conference on Uncertainty in Artificial Intelligence*, UAI'13, 172–181.
- [9] Colombo, D. and Maathuis, M. (2014) Order-independent constraint-based causal structure learning. *J. Mach. Learn. Res.*, **15**, 3741–3782.
- [10] Colombo, D., Maathuis, M. H., Kalisch, M. and Richardson, T. S. (2012) Learning high-dimensional directed acyclic graphs with latent and selection variables. *Ann. Statist.*, **40**, 294–321.
- [11] Darnell, J. E. (2002) Transcription factors as targets for cancer therapy. *Nature Reviews Cancer*, **2**, 740–749.
- [12] Drton, M. and Maathuis, M. H. (2017) Structure learning in graphical modeling. *Annual Review of Statistics and Its Application*, **4**, 365–393.

- [13] Eeckhoutte, J., Métivier, R. and Salbert, G. (2009) Defining specificity of transcription factor regulatory activities. *Journal of Cell Science*, **122**, 4027–4034.
- [14] Foygel, R. and Drton, M. (2010) Extended bayesian information criteria for gaussian graphical models. In *Advances in Neural Information Processing Systems 23*, 604–612.
- [15] Frot, B., Jostins, L. and McVean, G. (2017) Latent variable model selection for Gaussian conditional random fields. Available at: arXiv:1512.06412.
- [16] Gagnon-Bartsch, J. A., Jacob, L. and Speed, T. P. (2013) Removing unwanted variation from high dimensional data with negative controls. *Tech. Rep. 820*, Department of Statistics, University of California at Berkeley.
- [17] Van de Geer, S. and Bühlmann, P. (2013) ℓ_0 -penalized maximum likelihood for sparse directed acyclic graphs. *Ann. Statist.*, **41**, 536–567.
- [18] Han, H., Shim, H., Shin, D., Shim, J. E., Ko, Y., Shin, J., Kim, H., Cho, A., Kim, E., Lee, T., Kim, H., Kim, K., Yang, S., Bae, D., Yun, A., Kim, S., Kim, C. Y., Cho, H. J., Kang, B., Shin, S. and Lee, I. (2015) TRRUST: a reference database of human transcriptional regulatory interactions. *Scientific Reports*, **5**.
- [19] Han, S. W., Chen, G., Cheon, M.-S. and Zhong, H. (2016) Estimation of directed acyclic graphs through two-stage adaptive lasso for gene network inference. *J. Am. Statist. Ass.*, **111**, 1004–1019.
- [20] Harris, N. and Drton, M. (2013) PC algorithm for nonparanormal graphical models. *J. Mach. Learn. Res.*, **14**, 3365–3383.
- [21] Hastie, T., Tibshirani, R. and Wainwright, M. (2015) *Statistical Learning with Sparsity: The Lasso and Generalizations*. Boca Raton, USA: Chapman & Hall/CRC.
- [22] Heinze-Deml, C., Maathuis, M. H. and Meinshausen, N. (2018) Causal structure learning. To appear. Available at: arXiv:1706.09141.
- [23] Kalisch, M. and Bühlmann, P. (2007) Estimating high-dimensional directed acyclic graphs with the PC-algorithm. *J. Mach. Learn. Res.*, **8**, 613–636.
- [24] Kalisch, M., Mächler, M., Colombo, D., Maathuis, M. and Bühlmann, P. (2012) Causal inference using graphical models with the R package pcalg. *J. Statist. Software*, **47**, 1–26.
- [25] Leek, J. T. and Storey, J. D. (2007) Capturing heterogeneity in gene expression studies by surrogate variable analysis. *PLoS Genetics*, **3**, e161.
- [26] Ma, S., Xue, L. and Zou, H. (2013) Alternating direction methods for latent variable gaussian graphical model selection. *Neural Comput.*, **25**, 2172–2198.
- [27] Maathuis, M. H., Colombo, D., Kalisch, M. and Bühlmann, P. (2010) Predicting causal effects in large-scale systems from observational data. *Nature methods*, **7**, 247–8.
- [28] Maathuis, M. H., Kalisch, M. and Bühlmann, P. (2009) Estimating high-dimensional intervention effects from observational data. *Ann. Statist.*, **37**, 3133–3164.
- [29] Malinsky, D. and Spirtes, P. (2016) Estimating causal effects with ancestral graph Markov models. In *Proceedings of the Eighth International Conference on Probabilistic Graphical Models*, vol. 52 of *Proceedings of Machine Learning Research*, 299–309. Lugano, Switzerland: PMLR.
- [30] Mostafavi, S., Battle, A., Zhu, X., Urban, A. E., Levinson, D., Montgomery, S. B. and Koller, D. (2013) Normalizing RNA-sequencing data by modeling

- hidden covariates with prior knowledge. *PLoS ONE*, **8**, e68141.
- [31] Nandy, P., Hauser, A. and Maathuis, M. H. (2017) High-dimensional consistency in score-based and hybrid structure learning. Available at: arXiv:1507.02608.
- [32] Nandy, P., Maathuis, M. H. and Richardson, T. S. (2017) Estimating the effect of joint interventions from observational data in sparse high-dimensional settings. *Ann. Statist.*, **45**, 647–674.
- [33] Pearl, J. (2009) Causal inference in statistics: an overview. *Statistics Surveys*, **3**, 96–146.
- [34] — (2009) *Causality: Models, Reasoning and Inference*. Cambridge: Cambridge University Press, 2nd edn.
- [35] Ravikumar, P. K., Raskutti, G., Wainwright, M. J. and Yu, B. (2009) Model selection in Gaussian graphical models: High-dimensional consistency of l_1 -regularized mle. In *Advances in Neural Information Processing Systems 21*, 1329–1336. Curran Associates, Inc.
- [36] Redell, M. and Tweardy, D. (2005) Targeting transcription factors for cancer therapy. *Current Pharmaceutical Design*, **11**, 2873–2887.
- [37] Richardson, T. S. and Spirtes, P. (2002) Ancestral graph Markov models. *Ann. Statist.*, **30**, 962–1030.
- [38] Robinson, R. W. (1977) *Counting unlabeled acyclic digraphs*, 28–43. Combinatorial Mathematics V: Proceedings of the Fifth Australian Conference. Springer Berlin Heidelberg.
- [39] Shpitser, I., Evans, R. J., Richardson, T. S. and Robins, J. M. (2013) Sparse nested markov models with log-linear parameters. In *Proceedings of the Twenty-Ninth Conference on Uncertainty in Artificial Intelligence*, UAI'13, 576–585.
- [40] Spirtes, P., Glymour, C. and Scheines, R. (2000) *Causation, Prediction, and Search*. Adaptive Computation and Machine Learning. Cambridge: MIT Press, second edn.
- [41] Spirtes, P., Meek, C. and Richardson, T. (1995) Causal inference in the presence of latent variables and selection bias. In *In Proceedings of Eleventh Conference on Uncertainty in Artificial Intelligence*, 499–506. San Francisco, CA: Morgan Kaufmann.
- [42] Stegle, O., Parts, L., Piipari, M., Winn, J. and Durbin, R. (2012) Using probabilistic estimation of expression residuals (PEER) to obtain increased power and interpretability of gene expression analyses. *Nature Protocols*, **7**, 500–507.
- [43] Tsamardinos, I., Brown, L. E. and Aliferis, C. F. (2006) The max-min hill-climbing Bayesian network structure learning algorithm. *Mach. Learn.*, **65**, 31–78.
- [44] Verma, T. and Pearl, J. (1991) Equivalence and synthesis of causal models. In *Proceedings of the Sixth Annual Conference on Uncertainty in Artificial Intelligence*, UAI '90, 255–270. New York, NY, USA: Elsevier Science Inc.
- [45] Wille, A., Zimmermann, P., Vranová, E., Fürholz, A., Laule, O., Bleuler, S., Hennig, L., Prelić, A., von Rohr, P., Thiele, L., Zitzler, E., Gruissem, W. and Bühlmann, P. (2004) Sparse graphical Gaussian modeling of the isoprenoid gene network in arabidopsis thaliana. *Genome Biology*, **5**, R92.
- [46] Zhang, J. (2008) On the completeness of orientation rules for causal discovery in the presence of latent confounders and selection bias. *Artificial Intelligence*,

172, 1873–1896.

- [47] Zou, H. (2006) The adaptive lasso and its oracle properties. *J. Am. Statist. Ass.*, **101**, 1418–1429.

SEMINAR FÜR STATISTIK, ETH ZÜRICH, ZÜRICH, SWITZERLAND

DEPARTMENT OF BIostatISTICS AND EPIDEMIOLOGY, UNIVERSITY OF PENNSYLVANIA, PHILADELPHIA, USA

SEMINAR FÜR STATISTIK, ETH ZÜRICH, ZÜRICH, SWITZERLAND

Current address: Marloes H. Maathuis, Seminar für Statistik, ETH Zürich, Zürich, Switzerland

E-mail address: `maathuis@stat.math.ethz.ch`